nature catalysis

Article

https://doi.org/10.1038/s41929-023-00967-8

Zeolites as equilibrium-shifting agents in shuttle catalysis

Received: 12 May 2022

Accepted: 11 May 2023

Published online: 08 June 2023

Check for updates

Jesse Dallenes[1], Jonas Wuyts[1], Niels Van Velthoven[1], Andraž Krajnc[2], Gregor Mali[2], Oleg A. Usoltsev[3], Aram L. Bugaev[4] & Dirk De Vos[1]

The catalytic shuttling of functional moieties has emerged as a promising strategy to substitute and diversify traditional hydrofunctionalization technologies. However, these reactions are reversible due to their isodesmic nature, which limits their applicability to a select array of donor and acceptor molecules, and poses substantial challenges with regard to atom economy and practicality. Here we show an approach that harnesses the shape-selective and catalytic properties of zeolites to drive the shuttling equilibrium of transfer hydrocyanation and transfer hydroformylation reactions to near-completion. The zeolites irreversibly convert the transfer reaction co-products in an exergonic tandem reaction while excluding the substrates via pore size restrictions. Through fine-tuning of the zeolite's properties, yield increases of up to 80% can be achieved, enabling diversification of nitrile donors to propionitrile and aldehyde acceptors to unactivated olefins. Mechanistic and spectroscopic studies highlight the unique synergy between the zeolites and the homogeneous transfer catalysts.

Hydrofunctionalization of olefins is a fundamental process in the chemical industry[1]. Chemical functionalities are typically introduced from simple reactants such as HCN, H_2/CO, HCl, HF, H_2S and B_2H_6, which are all notoriously toxic, corrosive, flammable and volatile. Avoiding these reactants requires impractical and time-consuming multi-step detours. Surrogates that release the compound in situ can be used, but many of these lead to equally toxic reaction environments. As a safer alternative, the catalytic transfer of hazardous functional groups has been proposed[2–4]. This strategy, coined shuttle catalysis by Morandi, has been demonstrated for cyanide, formyl and acid chloride transfer processes[5–7]. The array of interchangeable functional groups is steadily expanding, making it an exciting and dynamic field in homogeneous catalysis[8–18].

Perhaps the most distinctive feature of catalytic transfer reactions is their reversibility, inherent to the fact that the same types of molecules and bonds are present on either side of the reaction equation[2]. This implies the need for a driving force pushing the reaction to the desired side (Fig. 1a). Accordingly, suitable donor and/or acceptor molecules have to be selected or designed. For example, donors that undergo a substantial release of energy, or for which the reverse pathway is kinetically disfavoured, shift the equilibrium in the desired direction[7,19–21]. As a result, effective donors are restricted by specific structural requirements to a small selection of expensive molecules. Complementarily, selective removal of one product can drive the equilibrium, for example, via polymer precipitation or evaporation of low-boiling olefins, as in olefin metathesis[22]. In situ physical separation may be impractical or unsafe, for example, when flammable gases like lower olefins are to be removed[23]. Moreover, a physical separation can only influence the reaction equilibrium if the inherent reaction energetics are favourable, as is the case for exergonic reactions. On the contrary, a typical dehydrofunctionalization reaction is endergonic, emphasizing the need for co-products privileged by thermodynamic stability[5,19,20,24] or the use of highly reactive acceptors[6,7,13,14,25]. Two key shuttle reactions exemplify these restrictions. First, transfer hydrocyanations rely on a limited set of HCN donors, the performance of which is governed by thermodynamics. As a consequence, atom-economic

[1]Centre for Membrane Separations, Adsorption, Catalysis, and Spectroscopy for Sustainable Solutions (cMACS), KU Leuven, Leuven, Belgium. [2]Department of Inorganic Chemistry and Technology, National Institute of Chemistry, Ljubljana, Slovenia. [3]The Smart Materials Research Institute, Southern Federal University, Rostov-on-Don, Russia. [4]Paul Scherrer Institute, Villigen, Switzerland. e-mail: dirk.devos@kuleuven.be

https://doi.org/10.1038/s41929-023-00967-8

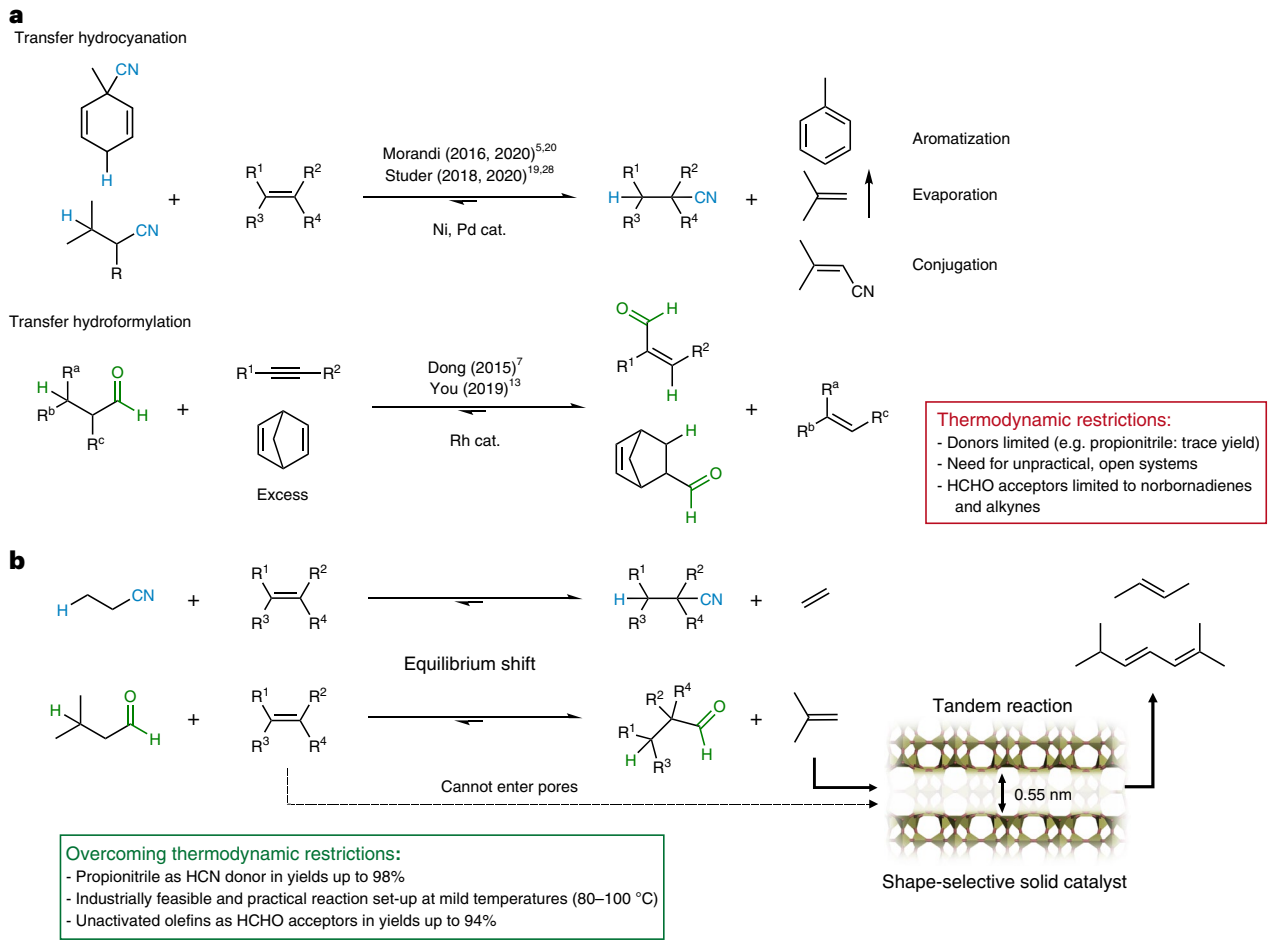

Fig. 1 | Driving the equilibrium of catalytic shuttle reactions. a, Established paradigms for manipulating the reaction equilibrium. **b**, This work: shape-selective zeolite catalysts as equilibrium-shifting agents.

and industrially relevant donors such as propionitrile fail to give satisfactory results, as forming ethylene is thermodynamically uphill[5]. Second, the few reported transfer hydroformylations exclusively use highly reactive acceptors such as norbornadienes and alkynes, which are also used in excess to achieve optimal results[7,13]. Hence, a practical HCHO transfer to create value-added aldehydes from unactivated alkenes would be extremely beneficial[26]. To overcome these thermodynamic hurdles, we envisioned that the selective consumption of the small olefin co-products in a consecutive exergonic reaction, via concurrent tandem catalysis, might serve as an efficient overall driving force (Fig. 1b)[27].

However, several challenges have to be overcome. First, the olefin co-product must be selectively converted over the olefin substrate to drive the equilibrium. Second, the consecutive reaction must not interfere with the catalyst of the transfer reaction. Third, the products of the consecutive reaction should not compete with the olefin substrate of the transfer reaction. We hypothesized that the addition of a solid microporous catalyst to the reaction mixture might offer an elegant solution (Fig. 1b). If the pore windows of the catalyst are sufficiently narrow, the small olefin co-product should be able to diffuse efficiently into the pores of the catalyst and react, while the larger olefin substrate should be excluded. In addition, the active sites in the shape-selective solid catalyst should be physically separated from the homogeneous transfer catalyst. Finally, the solid catalyst should convert the olefin co-products into less reactive substrates for functional group transfer catalysis. In this Article we show the validity of these hypotheses by rationally designing and selecting zeolites as equilibrium-shifting agents for HCN and HCHO transfer reactions. Our strategy drastically improves the yields of these reactions, as demonstrated in over 50 examples, and is readily amenable to upscaling through its practical set-up, fostering future industrial application.

Results

Benchmark HCN transfer reactions without zeolite

Since the first report on the transfer hydrocyanation reaction in 2016, Ni, Pd and Co catalysts have been developed[5,19,20,25,28–31]. Lewis acid-mediated systems generate hydrocyanated alkenes with anti-Markovnikov selectivity, and are the most active because both oxidative addition and reductive elimination can be facilitated by the Lewis acid[32]. With $Ni(COD)_2$ or $NiCl_2$, DPEphos and $AlMe_2Cl$ as the catalytic system, isovaleronitrile and butyronitrile can be used as HCN donors, producing isobutene and propene as volatile and thermodynamically stable co-products[5,30]. In our initial catalyst screening, $Pd(OAc)_2$ combined with Xphos and $AlMe_2Cl$ proved to be a better catalyst system for small nitrile donors, affording yields of up to 25% with propionitrile as the HCN donor/solvent (Supplementary Tables 2–4). In an open system, with ethylene evaporation, the yield slightly improves to 30%. Although fairly poor, this result affirms the feasibility of using propionitrile as the HCN donor, and simultaneously highlights the strict thermodynamic limitations under which the standard reaction operates (Supplementary Tables 5 and 6).

https://doi.org/10.1038/s41929-023-00967-8

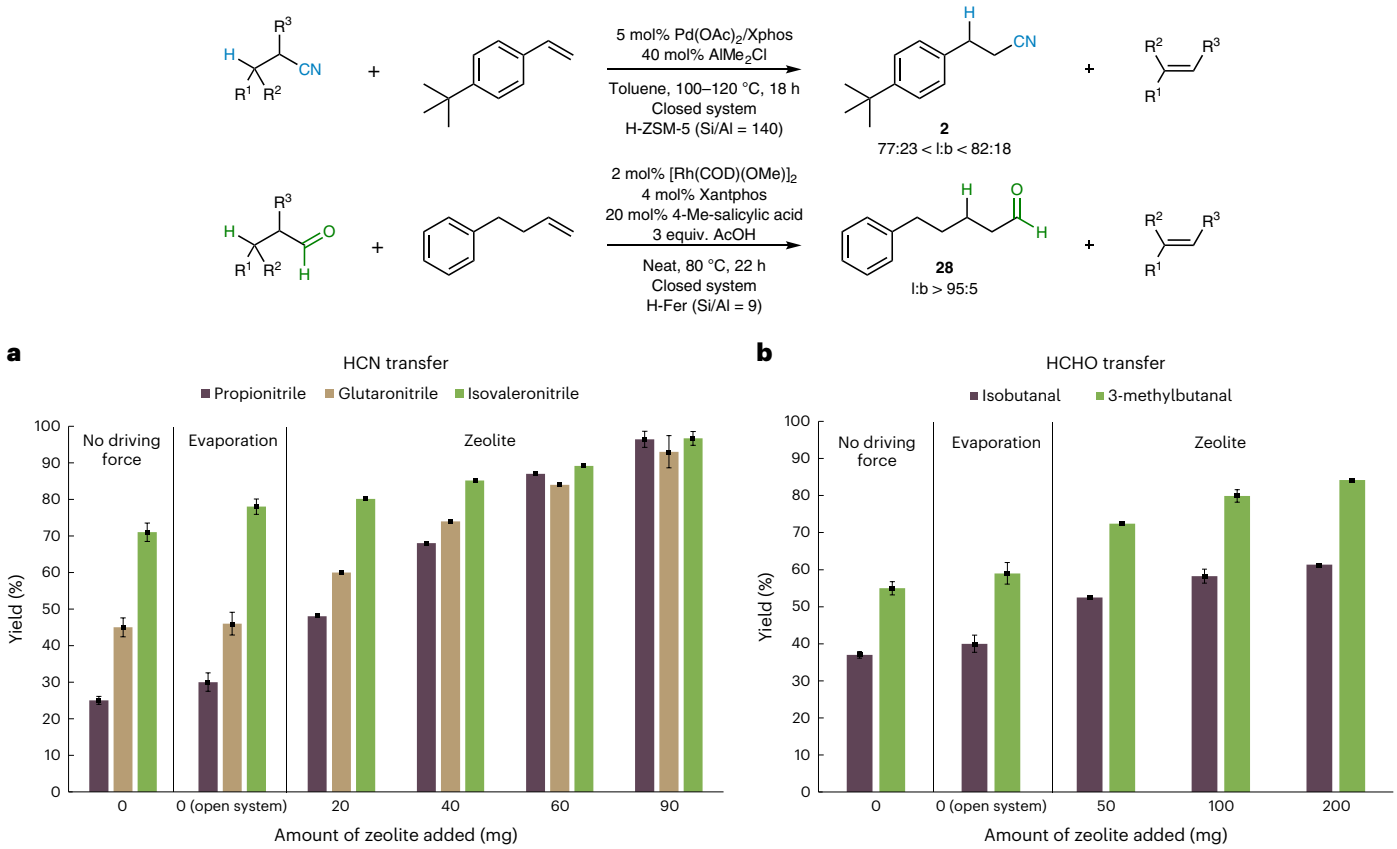

Fig. 2 | Effect of zeolites on reaction performance. a,**b**, Comparison of nitrile (**a**) and aldehyde (**b**) donors in HCN and HCHO transfer reactions without zeolite, with evaporation (reaction conducted under flowing Ar) and with zeolites: H-ZSM-5 with Si/Al = 140 for HCN transfer, H-FER with Si/Al = 9 for HCHO transfer. Reactions were performed on a 0.25-mmol scale in glass reaction vials. Reactions with isovaleronitrile and glutaronitrile were conducted with 5-equiv. nitrile in 0.5 ml of toluene at 120 °C. Reactions with propionitrile were conducted with 0.5 ml of propionitrile as solvent at 100 °C. Reactions with isobutanal and 3-methylbutanal were performed with 0.8 ml of the corresponding aldehyde as solvent at 80 °C. Yield is determined as the sum of the isomers via GC with 1,3,5-tri-*tert*-butylbenzene as internal standard. Error bars correspond to the s.d. of four independent measurements, and the data are represented as mean values ± s.d.

Benchmark HCHO transfer reactions without zeolite

The transfer hydroformylation reaction was first reported by Dong in 2015[7], although earlier studies by Brookhart laid out the prospect for such a reaction[33]. A Rh/Xantphos catalyst is used in cooperation with a benzoate counterion, which acts as a proton shuttle, facilitating de- and reprotonation of the Rh complex. The system was initially applied exclusively to the dehydroformylation of valuable aldehyde feedstocks using norbornadiene as a sacrificial HCHO acceptor. Later, the same catalyst system was used in a forward transfer hydroformylation of alkynes, with butyraldehyde as sacrificial HCHO donor[13]. However, as the alkyne needs to be used in excess, the practicality with regard to industrial application is fairly limited. Theoretical studies reaffirmed the apparent need for an activated acceptor (for example, strained olefin or alkyne) to drive the reaction to completion[21]. We therefore aimed to challenge this notion via our zeolite-based equilibrium-shifting concept. As a benchmark, a model reaction using 4-phenyl-1-butene as an unactivated HCHO acceptor was investigated; this indicated that yields of up to 47% could be obtained when a small aldehyde donor is used as solvent (for example, propanal, butanal, 3-methylbutanal, pentanal; Supplementary Table 7). Through further tweaking of the carboxylate counterion, the reaction conditions and the use of acetic acid as additive, the yield could be improved to 55% (Supplementary Table 8). Interestingly, styrenes could also be used as acceptors, but they require slightly higher reaction temperatures and work better with N-Xantphos as ligand (Supplementary Table 9).

Zeolites as equilibrium-shifting agents

With this frame of reference, we started out by exploring the validity of our equilibrium-shifting concept by adding microporous zeolite catalysts. We initially aimed at solids containing transition metals or acid sites, as these could lead to the selective production of internal olefin dimers and trimers[34–41]. For each transfer reaction, an extensive list of zeolites with various pore sizes and acidity was screened (Supplementary Tables 10 and 13). In the HCN transfer reaction with isovaleronitrile as donor and 4-*tert*-butylstyrene as acceptor, medium-pore zeolites (with 10-membered rings; 10-MR) with high Si/Al ratio (≥100), such as H-ZSM-5 (MFI), H-ZSM-48 (*MRE) and H-ZSM-11 (MEL), clearly increased the yield of the HCN transfer reaction compared to the zeolite-free benchmark. In contrast, the addition of zeolites with more Al or with large pore sizes (for example, 12-MR) resulted in a decrease of the yield. A straightforward explanation is found in the sensitivity and small kinetic diameter of the $AlMe_2Cl$ Lewis acid; low Si/Al zeolites contain larger amounts of hydroxyl groups, which react with the electrophilic Lewis acid. Indeed, inductively coupled plasma (ICP) and ^{27}Al magic-angle spinning (MAS) NMR measurements show up to threefold increases in the zeolite Al-contents (Supplementary Table 24). As the Lewis acid is needed for the HCN transfer reaction, its consumption deteriorates the reaction performance (Supplementary Table 11). To our delight, the commercially available H-ZSM-5 with Si/Al = 140 and 10-MR hits the sweet spot between minimizing unwanted Lewis acid consumption and maximizing the shape-selective conversion of the

https://doi.org/10.1038/s41929-023-00967-8

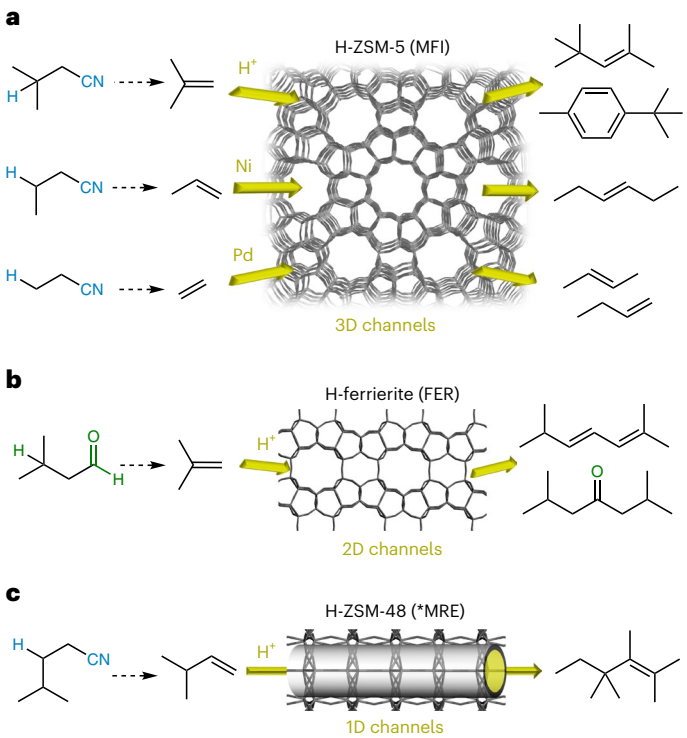

Fig. 3 | Tandem reactions catalysed by zeolites containing acid and/or transition metal sites. Topology, pore structure and catalytic sites can be rationally fine-tuned based on olefin size and reactivity. **a**, A 3D MFI pore structure decorated with acid and transition metal sites for the dimerization of isobutene, propene and ethylene. **b**, Two-dimensional (2D) FER topology in the acid-catalysed Prins condensation between 3-methylbutanal and isobutene. **c**, 1D pore channels of *MRE in the acid-catalysed dimerization of 3-methyl-1-butene.

alkene co-product (Fig. 2a). The reaction yield with multiple small and medium-sized ($\leq C_6$) nitrile donors shows substantial improvements with increasing amounts of H-ZSM-5 (Supplementary Fig. 3). Most notably, with propionitrile as HCN donor and solvent, the reaction with zeolite achieves nearly quantitative conversion (yield = 96%), compared to merely 30% without zeolite in an open system. When larger nitrile donors are used (for example, 3-phenylpropionitrile), the zeolite has little to no effect, which hints at shape-selectivity. Kinetic experiments clearly visualize the beneficial effect of H-ZSM-5, showing that the reaction immediately stalls when the zeolite is removed at any point (Supplementary Fig. 14).

In the transfer hydroformylation reaction with small, branched aldehydes as donors (isobutanal, 3-methylbutanal) and 4-phenyl-1-butene as acceptor, the yield clearly increases with the addition of acid zeolites, among which H-ferrierite (FER, Si/Al = 9) is most effective (Supplementary Table 13). For example, the HCHO transfer reaction yield with 3-methylbutanal as donor could be increased from 55% to 80% by adding 100 mg of H-FER (Fig. 2b). As most of the remaining 4-phenyl-1-butene is hydrogenated, the equilibrium appears to be fully shifted to the right. For comparison, the same reaction without zeolite in an open system with evaporation affords no substantial improvement (Fig. 2b). With linear aldehydes as donors (propanal, butanal, pentanal), the yield decreases in the presence of acid zeolites (Supplementary Table 13), probably due to the formation of aldehyde self-condensation products, which appear to poison the HCHO transfer catalyst (Supplementary Figs. 18 and 19). With branched aldehydes, minimal to even no condensation products were observed. Moreover, these aldehydes provide a convenient tandem reaction pathway by shape-selectively reacting with their olefin co-product over an acid zeolite catalyst in a Prins reaction[42–44].

Mapping the zeolite reaction networks

In the HCN transfer reaction with H-ZSM-5, the zeolite transforms the olefin co-products derived from medium-sized HCN donors (C_4–C_6) to a plethora of higher olefins, presumably via dimerization and trimerization reactions (propene reacts to 2-methyl-2-pentene and other hexenes; isobutene reacts to diisobutylene isomers and so on; Fig. 3 and Supplementary Table 12). The common thread for this group of donors is the formation of mono-, di- or tri-substituted alkene co-products, which are highly reactive when exposed to acidic zeolites[45–50]. Control reactions with the neat olefin co-products unequivocally confirmed the oligomerization activity of the acid zeolite (Supplementary Figs. 24–29). In the presence of $AlMe_2Cl$, the isobutene and propene conversions are noticeably higher, suggesting that the Lewis acid might generate additional acidity in the zeolite (Supplementary Figs. 24 and 25)[51–53]. With propionitrile as a donor, highly selective dimerization of ethylene was observed (*trans*-2-butene > 1-butene > *cis*-2-butene; Fig. 3). Moreover, hydrocyanated butenes, that is, 2-methylbutanenitrile and valeronitrile, appeared in considerable quantities. In contrast to substituted alkenes, ethylene is not dimerized over an acid zeolite at mild reaction temperatures and low ethylene concentrations (Supplementary Figs. 26 and 28)[40,41]. This implies that ethylene must be converted inside the zeolite by a different mechanism from the other olefins. Control experiments showed that with the sole addition of $Pd(OAc)_2$ and H-ZSM-5 to the reaction mixture, butenes were formed from ethylene at 100 °C in high selectivities (C_4 > 96%; Supplementary Figs. 26–29). This firmly indicates that the Pd(II)-loaded zeolite is the active ethylene dimerization catalyst.

In line with the HCN transfer reaction with isovaleronitrile and H-ZSM-5, small amounts of diisobutylene and related isomers could be detected after the HCHO transfer reaction with 3-methylbutanal as donor and H-FER as zeolite. However, larger amounts of additional products were observed, such as unsaturated C_9H_{16} hydrocarbons (for example, 2,6-dimethyl-2,4-heptadiene) and a ketone (2,6-dimethyl-4-heptanone) (Fig. 3b and Supplementary Table 17). These products are formed via the Prins reaction between 3-methylbutanal and isobutene, initially leading to an α,β-unsaturated alcohol intermediate that can undergo dehydration to a diene, or isomerization to the enol followed by keto-enol tautomerization, resulting in a ketone[43]. Moreover, a substantial fraction of the isobutene-derived products appears to remain inside the zeolite pores, probably due to adsorption and diffusion constraints, or in the form of coke (Supplementary Fig. 34).

Fine-tuning the zeolite for different donors/acceptors

The selection and design of the zeolites as equilibrium-shifting agents can be rationalized by maximizing their reactivity with the olefin co-products (Fig. 3). For example, decorating H-ZSM-5 with Ni centres leads to a more active propene dimerization catalyst, resulting in a larger equilibrium-shifting effect in the HCN transfer reaction (Supplementary Figs. 4 and 25). When using H-ZSM-48 (*MRE, Si/Al = 100), which has a one-dimensional (1D) pore channel structure, the formation of large, bulky olefins is possibly retarded[54–57]. As a result, H-ZSM-48 displays a larger equilibrium-shifting effect with nitrile donors that produce branched olefins, which are prone to the formation of bulky oligomers (isocapronitrile, isovaleronitrile), compared to the H-ZSM-5 zeolite with its more spacious three-dimensional (3D) pore channel structure (Supplementary Fig. 5 and Supplementary Table 10). A similar effect may explain why H-FER outperforms other 10-MR zeolites in the HCHO transfer reaction, as the ferrierite channels are more constrained, limiting, for example, 3-methylbutanal self-condensation. However, when the HCHO transfer is conducted with styrenes as substrates at higher temperatures, H-ZSM-5 performs better than H-FER (Supplementary Table 16). This could be the result of a kinetic effect, whereby the faster isobutene conversion in H-ZSM-5 can better keep up with the faster styrene conversion (compared to the

https://doi.org/10.1038/s41929-023-00967-8

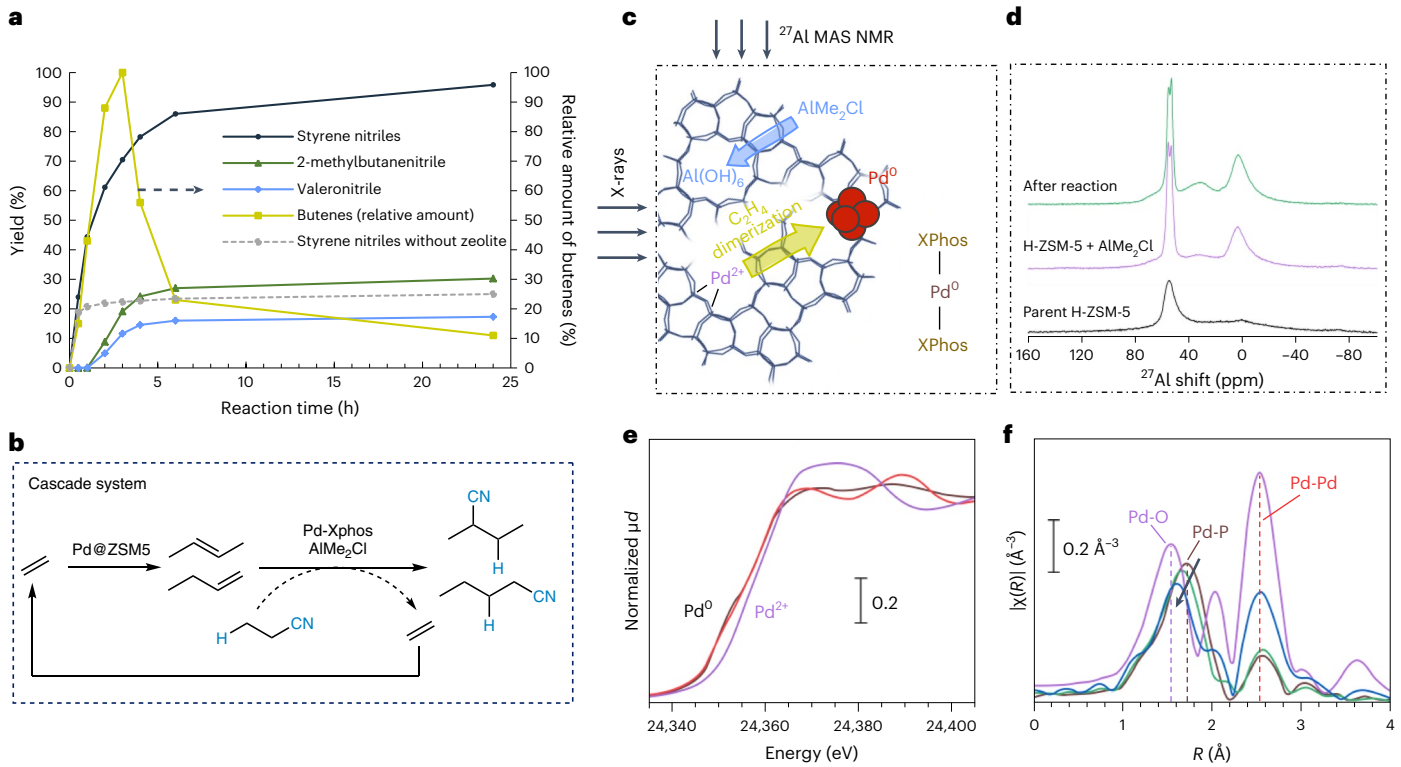

Fig. 4 | Mechanistic and spectroscopic studies of H-ZSM-5-assisted transfer hydrocyanation with propionitrile. a, Time profiles of butenes (sum of 1-butene and 2-butenes), C_5-nitriles (valeronitrile and 2-methylbutanenitrile) and styrene nitriles (sum of linear and branched products) in standard transfer hydrocyanation with zeolite (solid lines) and in the absence of zeolite (dotted line; only styrene nitriles are formed). Relative amount of butenes = $100 \times \text{mmol}_{\text{butenes}, t=x}/\text{mmol}_{\text{butenes, max}}$. **b**, Tandem reactions starting from ethylene. **c**, Schematic overview of the characterization tools used to identify Pd and Al-species. **d**, ^{27}Al MAS NMR spectra of the parent H-ZSM-5 (black), H-ZSM-5 zeolite preloaded in propionitrile with addition of $AlMe_2Cl$ (purple) and H-ZSM-5 after transfer hydrocyanation reaction (green). **e**, XANES data for ZSM-5 preloaded with $Pd(OAc)_2$ in toluene (purple), $Pd(OAc)_2$ dissolved in propionitrile in the presence of XPhos (brown) and recovered zeolite after an HCN transfer reaction (red). **f**, In situ EXAFS data for samples at the end of reaction with XPhos:zeolite ratios (in mol%:mg) of 0:100 (purple), 2.5:90 (blue), 5:90 (green) and 5:0 (brown).

slower 4-phenyl-1-butene reaction), thus maximizing the synergistic effect of the tandem reaction.

In-depth study of the propionitrile/H-ZSM-5 system

The interplay between the homogeneous catalyst and the zeolite was investigated using the HCN transfer reaction with propionitrile and H-ZSM-5 as a model system, as it gave the most impressive gains in yield (up to 80%). To disentangle the kinetic and thermodynamic reaction characteristics, the kinetics and the effect of increased zeolite loadings were monitored separately. The time profile displays a transient appearance of butenes followed by C_5 nitriles, while the hydrocyanated styrene products are formed from the onset of the reaction in quasi first-order kinetics (Fig. 4a,b). As expected, the zeolite has little influence on the kinetics, but clearly shifts the plateau yield of the styrene nitrile products to a higher level (Supplementary Figs. 13 and 30). This equilibrium-shifting effect can be related to a change of the molar reaction free energy, due to the coupling of the transfer hydrocyanation reaction with the ensuing dimerization. This $\Delta(\Delta_r G°)$ can be calculated from the reaction data. Theoretical DFT calculations validate the empirical values, which are sufficiently large ($\Delta(\Delta_r G°) \approx -30$ kJ mol^{-1}) to justify the experimental increases in yield (Supplementary Discussion). Although the zeolite's beneficial effect is grounded in thermodynamics, the kinetics of the coupled reaction must still be favourable for fully valorizing the equilibrium-shifting effect. With propionitrile, the reaction is initially moderately fast, but thanks to the continuous conversion of ethylene by the zeolite, the formation of the hydrocyanated product is continued at the same rate, well beyond the styrene conversion level that would be the thermodynamic limit in the absence of the zeolite (compare the dark blue and dotted grey curves in Fig. 4a). With the other, more reactive nitrile donors, the conversion quickly reaches the normal equilibrium level, which in the presence of the zeolite, gradually progresses up to higher levels (Supplementary Figs. 11–17).

A molecular picture of the active sites working in a concerted fashion was revealed via in situ and ex situ X-ray absorption near edge structure (XANES) and extended X-ray absorption fine structure (EXAFS) measurements (Fig. 4c,e,f). Ex situ XANES and EXAFS spectra of zeolites preloaded with $Pd(OAc)_2$ in toluene are consistent with a mononuclear square planar Pd(II)-zeolite species coordinated with four oxygen atoms, two from acetate and two from the zeolite (Fig. 4e, Supplementary Figs. 36 and 37 and Supplementary Table 25). Even when an equimolar amount of the reducing phosphine ligand Xphos is added, cationic Pd(II)-zeolite species are still formed inside the zeolite (Supplementary Fig. 38). Zeolites recovered after an HCN transfer reaction or an ethylene dimerization reaction show strikingly similar spectra, which can be assigned to subnanometric Pd(0)-carbide species (Supplementary Fig. 40 and Supplementary Table 26)[58]. The EXAFS spectra of in situ XAS measurements of the HCN transfer reaction are dominated by Pd–P contributions (Fig. 4f), originating from the catalyst complex $Pd(0)(Xphos)_2$ (that is, the resting state), along with smaller contributions of Pd–Pd interactions (Supplementary Fig. 41 and Supplementary Table 27). When H-ZSM-5 is added to the reaction, Pd–O species can be detected before, after and during the reaction, highlighting the presence of zeolite-bound Pd(II) in the ethylene dimerization catalyst (Supplementary Fig. 42 and Supplementary

https://doi.org/10.1038/s41929-023-00967-8

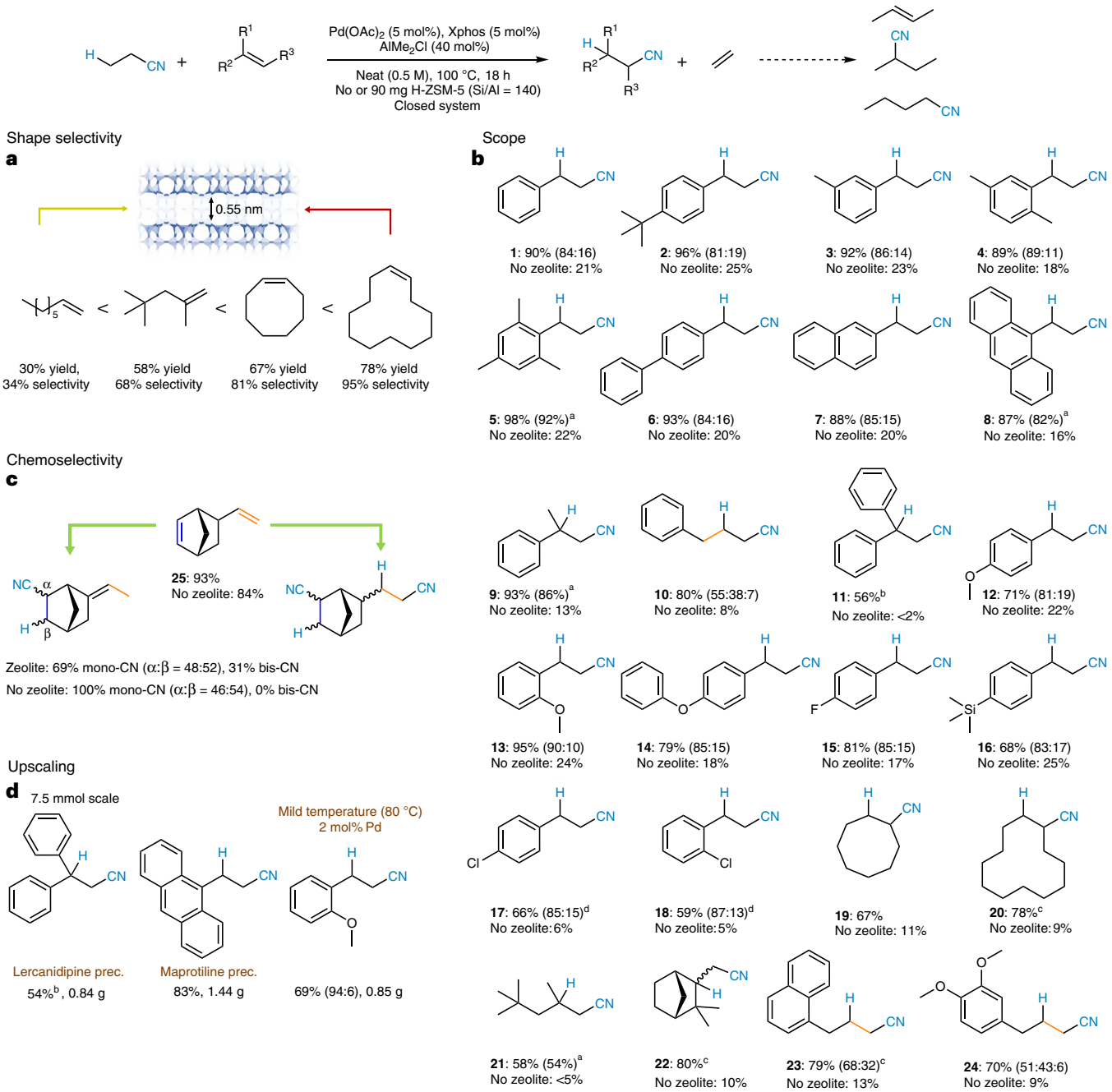

Fig. 5 | Substrate scope of the zeolite-assisted transfer hydrocyanation. **a**, Molecular sieving effect of the H-ZSM-5 zeolite in the transfer hydrocyanation of alkene substrates with varying kinetic diameters. **b**, Substrate scope of the zeolite-enhanced transfer hydrocyanation with propionitrile as HCN donor. **c**, Selective double-bond functionalization. **d**, Gram-scale synthesis of selected examples. Left two examples: standard reaction. Right: practical, gas- and reflux-free reaction at T = 80 °C with 2 mol% Pd/Xphos. All reactions were performed in propionitrile as solvent (0.5 M). GC yields using 1,3,5-tri-*tert*-butylbenzene as internal standard are reported. Linear-to-branched ratios are given in parentheses. [a]Isolated yields. [b]Reaction with 80 mol% $AlMe_2Cl$ and 200-mg H-ZSM-5 at T = 120 °C. [c]Reaction with 60 mol% $AlMe_2Cl$ and 150 mg H-ZSM-5 (T = 100 °C). [d]Reaction performed with Pd_2dba_3/CyJohnPhos as catalyst and a $Pd(OAc)_2$-loaded H-ZSM-5 zeolite (0.3 wt% Pd) (see Supplementary Methods for details).

Table 28). Moreover, the contribution of Pd–O species becomes more dominant when the Pd:Xphos ratio is increased to 2:1 (indicated by an arrow in Fig. 4f), as more Pd centres are able to migrate inside the zeolite due to the lower amount of Xphos in the solution. ICP data confirm this, showing a threefold increase in the zeolite Pd wt% at a Pd:Xphos ratio of 2:1 (Supplementary Table 24).

Finally, modifications of the zeolite's structure and acid characteristics were studied with powder X-ray diffraction (PXRD) and ^{27}Al MAS NMR. No loss of crystallinity could be observed via PXRD, confirming that the zeolite structure stays intact (Supplementary Fig. 33). The ^{27}Al MAS NMR spectrum of parent H-ZSM-5 shows a single peak at 55 ppm corresponding to the tetrahedrally coordinated framework aluminium (Fig. 4d)[59]. After contact with $AlMe_2Cl$ at room temperature or after a transfer hydrocyanation reaction, new signals appear at 5 and 35 ppm, with the former being dominant. Notably, no signature shifts of Al–CH_3 or Al–Cl bonds could be observed. The signal at 5 ppm corresponds to extra-framework aluminium that is octahedrally coordinated, and the one at 35 ppm can be assigned to pentahedral aluminium species[53].

https://doi.org/10.1038/s41929-023-00967-8

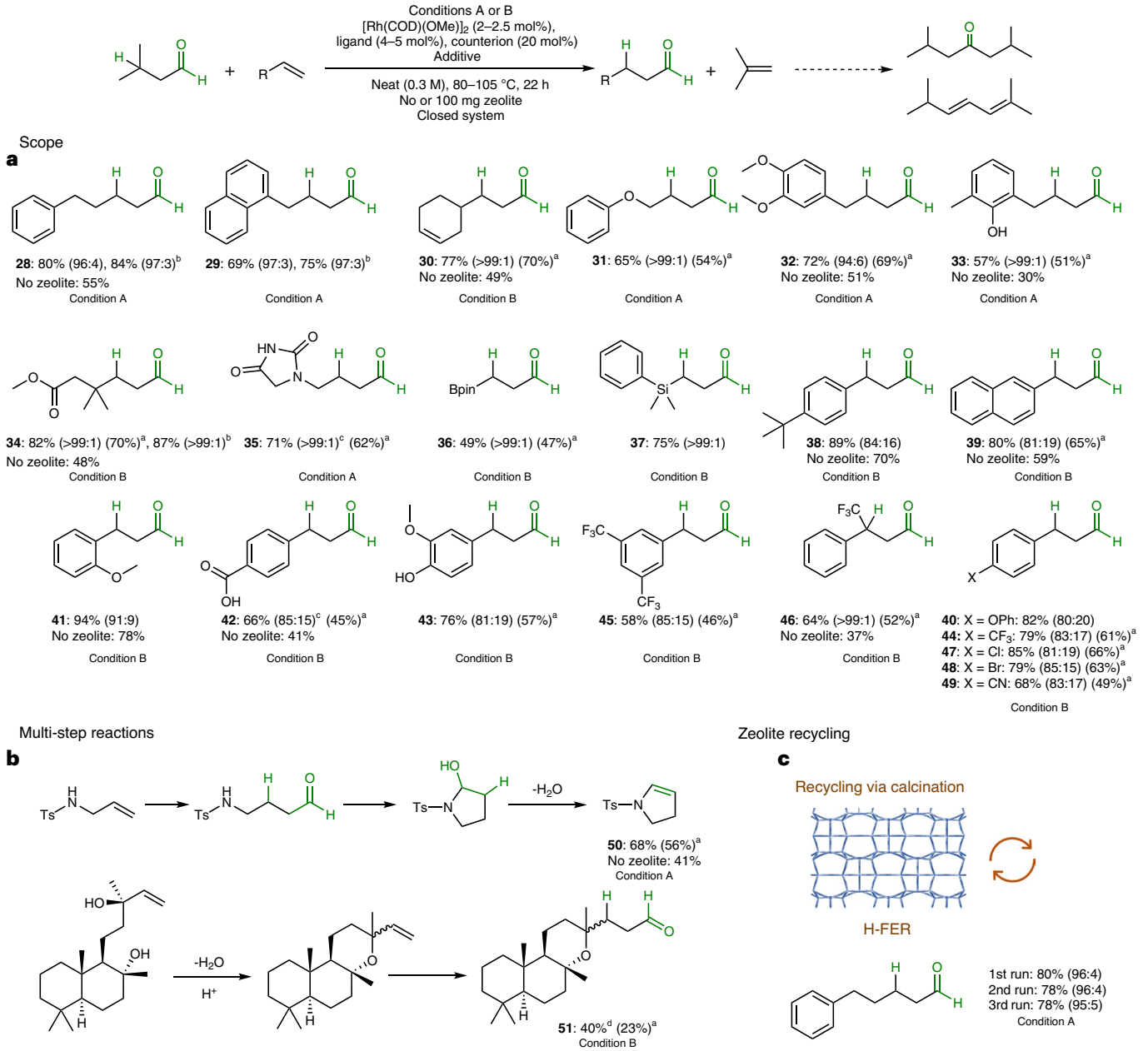

Fig. 6 | Substrate scope of the zeolite-assisted transfer hydroformylation. **a**, Scope of the zeolite-assisted transfer hydroformylation reaction. **b**, One-pot, multi-step hydroformylative transformations of allylic amine and sclareol. **c**, Recycling of the zeolite via calcination. GC yields using 1,3,5-tri-*tert*-butylbenzene as internal standard are reported. Linear-to-branched ratios are given in parentheses. Conditions A: 2 mol% Rh precatalyst, 4 mol% Xantphos, 20 mol% 4-methylsalicylic acid, 3 equiv. of AcOH, 80 °C, 100 mg H-FER (Si/Al = 9). Conditions B: 2.5 mol% Rh precatalyst, 5 mol% N-Xantphos, 20 mol% benzo[b]furan-2-carboxylic acid, 105 °C, 100 mg of H-ZSM-5 (Si/Al = 140). All reactions were performed in 3-methylbutanal as solvent (0.3 M). [a]Isolated yields of linear isomer. [b]Reaction with 200 mg of zeolite (100 mg for first 6 h reaction, then 100 mg for remaining 16 h). [c]NMR yield with 1,3,5-trimethoxybenzene as internal standard. [d]Trifluoroacetic acid was added to promote sclareol cyclization (see Supplementary Discussion for details).

Thus, $AlMe_2Cl$ appears to be hydrolysed inside the zeolite, which further corroborates the need for high Si/Al zeolites and slightly higher Lewis acid loadings. Residual silanol groups (Supplementary Fig. 46) and water molecules associated with the zeolite's acid sites may facilitate the hydrolysis process[53].

Substrate scope, upscaling and recycling

To assess the shape-selective nature of our concept, alkene substrates with varying kinetic diameters were employed (Fig. 5a and Supplementary Fig. 23). With 1-octene as substrate, the zeolite-assisted HCN transfer reaction showed high conversion of 1-octene, but low selectivity to the nitrile products, indicating octene diffusion inside the zeolite. The selectivity towards nitriles increased with the kinetic diameter of the corresponding alkene, thus firmly supporting the shape-selective nature of the system. With propionitrile as simple and cost-efficient HCN donor, the scope of the zeolite-assisted transfer hydrocyanation was explored (Fig. 5b). Various alkyl- and aryl-substituted styrenes (**1**–**8**) consistently show high yields (>87%), with remarkable increases of ~70% compared to the reactions without zeolite. The largest zeolite-induced increases in yield were observed for α-methylstyrene (**9**) (13 → 93%) and *trans*-β-methylstyrene (**10**) (8 → 80%). The system is compatible with fluoro-, alkoxy- and silyl-substituents (**12**–**16**). Chlorostyrenes

were initially problematic, presumably due to oxidative addition of the C–Cl bond by $Pd(OAc)_2$/Xphos[60]. However, combining the Cl-tolerant Pd_2dba_3/CyJohnPhos[61] with a preloaded Pd-ZSM-5 zeolite furnished the nitrile products of 4-chlorostyrene (**17**) and 2-chlorostyrene (**18**) in good yields. Aliphatic cyclic and branched alkenes with C ≥ 8 resulted in good yields (**19**–**22**). Allylarenes were also effective, albeit with moderate linear regioselectivities (**23**–**24**). A fascinating example is 5-vinyl-2-norbornene (**25**), which bears both an activated double bond and an unactivated one (Fig. 5c). The reaction without zeolite in propionitrile solely functionalizes the activated double bond, enabled by the exergonic strain release in norbornene. However, with the zeolite, a considerable fraction of dinitriles (31%) is also obtained, indicating sequential functionalization of the unactivated bond. Thus, for reactions of simple, non-strained alkenes, the Pd-zeolite-catalysed ethylene dimerization balances the (energetic) scales, allowing efficient transfer hydrocyanation. To further illustrate the large-scale practicality of our concept, reactions were performed on a 7.5-mmol scale. The nitrile products of 9-vinylanthracene and 1,1-diphenylethylene, which are precursors of pharmaceuticals such as maprotiline (an antidepressant) and lercanidipine (an antihypertensive)[62], could be obtained in good to excellent yield on a gram scale (Fig. 5d). For simple styrenes, the HCN transfer reaction with propionitrile works well at temperatures as low as 80 °C and with relatively low catalyst loadings (Fig. 5d). Such a closed system set-up, with practically no gas evolution or reflux, would be very attractive in a pharmaceutical setting.

Next, the zeolite-assisted transfer hydroformylation with 3-methylbutanal as HCHO donor was applied to a range of olefins (Fig. 6a). Using the optimized system of 4 mol% Rh/Xantphos, 20 mol% 4-methylsalicylic acid, 3 equiv. of AcOH with 100 mg H-FER zeolite (conditions A), several terminal, unactivated alkenes containing free hydroxyl groups, ethers, esters, internal double bonds and an imidazolidine-derived scaffold could be converted to the corresponding aldehydes in good to excellent yields (57–87%) and regioselectivities (linear:branched > 94:6) (**28**–**35**). Additionally, electronically diverse olefins such as vinyl boronates and vinyl silanes are susceptible to the reaction (**36**, **37**). The effect of the zeolite on the yield fluctuates between 17% and 39%, resulting in net yields of up to 87%, which makes our approach a viable alternative to traditional hydroformylation methods. Using a modified catalytic system consisting of 5 mol% Rh/N-Xantphos, 20 mol% benzo[b]furan-2-carboxylic acid and 100 mg of H-ZSM-5 (Si/Al = 140) (conditions B), styrenes could be converted into the corresponding linear aldehydes in yields of up to 94%. A diverse range of functional groups, such as ethers, unprotected alcohols and carboxylic acids, chlorides, bromides, cyanides and trifluoromethyls, including a challenging α-CF_3-styrene, were well tolerated (**38**–**49**). Furthermore, the flexibility of our method is demonstrated by a one-pot transfer hydroformylation-cyclization-dehydration sequence, converting tosyl-protected allyl amine into tosyl-protected 2-pyrroline (**50**) and sclareol into a hydroformylated manoyl oxide derivative (**51**) (Fig. 6b). Such schemes may incentivize the development of more complex synthetic pathways, building on the synergy between homogeneous metal complexes and solid acids as combined equilibrium-shifting agents and dehydration catalysts. Finally, the zeolite catalyst can be recycled via calcination, as the pores contain mostly organic material, justifying the use of higher zeolite amounts per reaction (Fig. 6c). From a process standpoint, this could open up possibilities for the use of packed bed reactors, enabling facile recovery of the stationary phase after reaction.

Conclusions

In summary, we have reported a strategy to overcome the thermodynamic limitations of catalytic transfer hydrocyanation and transfer hydroformylation reactions using shape-selective zeolite catalysts. The zeolite is tunable depending on the donor/acceptor combination, and leads to increases in yield of up to 80% for the HCN transfer and up to 39% for the HCHO transfer. Distinct types of zeolite-catalysed tandem reaction, such as Pd-catalysed ethylene dimerization, acid-catalysed oligomerizations and olefin-aldehyde Prins condensations emphasize the generality of this concept. Mechanistic and spectroscopic studies were used to unravel the zeolite-assisted transfer hydrocyanation with propionitrile, in which ethylene is dimerized by a Pd-zeolite species derived in situ from $Pd(OAc)_2$ and H-ZSM-5. The concept was further shown to be highly promising in the functionalization of industrially relevant substrates in a practical, upscalable and recyclable fashion. We believe that this zeolite-based equilibrium-shifting concept can serve as a blueprint for the development of advanced catalytic shuttle reactions.

Methods

HCN transfer reaction procedure

Generally, 2.81 mg of $Pd(OAc)_2$ (0.0125 mmol, ≥99.99% Merck), 5.95 mg of Xphos (0.0125 mmol), 90 mg of vacuum-activated H-ZSM-5 (Si/Al = 140, calcined CBV-28014) and 24.6 mg of 1,3,5-tri-*tert*-butylbenzene (0.1 mmol, internal standard) were added to a 1.5-ml glass vial. The vial was capped and subsequently flushed with Ar, after which Ar-flushed propionitrile (0.5 ml, 99% Merck) and olefin substrate (0.25 mmol) were added. Finally, 100 µl of 1 M $AlMe_2Cl$ in hexanes (or 110 µl of 0.9 M $AlMe_2Cl$ in heptanes) (0.1 mmol) was injected. The vial was then placed in a preheated aluminium heating block at 100 °C. After 18 h, the vial was cooled on ice, and two drops of methanol were added to quench residual Lewis acid. The solution was centrifuged and collected for analysis. Alternatively, syntheses were conducted in 0.5 ml of toluene as solvent, using 5–10 equiv. of nitrile donor at 120 °C. In some experiments, the amount of zeolite and Lewis acid was increased (in the same ratio).

HCHO transfer reaction procedure

Generally, 2.42 mg of $[Rh(OMe)(1,5\text{-cod})]_2$ (0.005 mmol), 5.78 mg of Xantphos (0.01 mmol), 6.1 mg of 4-methylsalicylic acid (0.05 mmol), 100 mg of H-FER (Si/Al = 9) and 24.6 mg of 1,3,5-tri-*tert*-butylbenzene (0.1 mmol, internal standard) were added to a 1.5-ml glass vial (conditions A). Alternatively, 2.42 mg of $[Rh(OMe)(1,5\text{-cod})]_2$ (0.005 mmol), 5.52 mg of N-Xantphos (0.01 mmol), 6.5 mg of benzo[b]furan-2-carboxylic acid (0.05 mmol), 100 mg of H-ZSM-5 (Si/Al = 140) and 24.6 mg of 1,3,5-tri-*tert*-butylbenzene (0.1 mmol, internal standard) were added to a 1.5-ml glass vial (conditions B). The glass vial was capped and put under an inert Ar atmosphere using a Schlenk line, after which Ar-flushed aldehyde (0.8 ml), acetic acid (40 µl, only for conditions A) and olefin substrate (conditions A, 0.25 mmol; conditions B, 0.2 mmol) were added. The vial was then placed in a preheated aluminium heating block at 80 °C (conditions A) or 105 °C (conditions B). After 22 h, the vial was cooled on ice. The zeolite was removed via centrifugation, and the products were analysed via gas chromatography flame ionization detection/gas chromatography mass spectrometry (GC-FID/GC-MS).

Reaction analysis

Product quantification was performed on a Shimadzu CP-Sil 5 CB column (Shimadzu GC-2010) equipped with a FID using 1,3,5-tri-*tert*-butylbenzene as an internal standard. The effective carbon number method was used to calculate the reaction yield, selectivities and conversions. Samples were automatically injected with a volume of 1 µl in split mode. The standard temperature program was 50 °C (5-min hold time), 10 °C min^{-1} to 200 °C, 12 °C min^{-1} to 300 °C and 8 °C min^{-1} to 325 °C (5-min hold time). An Agilent 6890 GC instrument with an HP-1 MS column and a 6973 MSD mass spectrometer was used for identification of the different products. ^1H and ^{13}C NMR spectra were recorded at 400 MHz and 101 MHz, respectively, using a Bruker Avance III HD 400 spectrometer, with $CDCl_3$ or DMSO-d_6 as the solvent. The data were analysed using the MestReNova 12.0.2 software package. Before NMR analysis, the solvent and low-boiling organics were evaporated under vacuum, and the products were extracted from an

acetonitrile/hexanes mixture. Some products were further purified by column chromatography.

Zeolite preparation and pretreating

Zeolites were obtained from commercial suppliers (for example, Zeolyst and Tosoh Europe) or synthesized via reported procedures. Zeolites in Na- or K-form (for example, K-Fer with Si/Al = 9, TSZ-720KOA from Tosoh Europe) were converted to their NH_4 form via exchange with NH_4NO_3 (0.5 M, 50 ml g^{-1} zeolite) three times at 80 °C, followed by washing and drying. Zeolites in NH_4 form (for example, CBV-28014 from Zeolyst) were calcined at T = 550 °C for 6 h using a temperature ramp of 2 °C min^{-1}. The H-form zeolites without incorporated transition metals were activated at 250 °C under vacuum (10^{-2} mbar) overnight, and subsequently stored under Ar in a dessicator before use. Zeolites with transition metals were activated in vacuo at room temperature. Metal catalysts were incorporated in the zeolites using the classic methods of ion exchange (0.1 M solution in water; for example, Ni-H-ZSM-5) or impregnation (0.005 M solution in toluene; for example, Pd-H-ZSM-5).

X-ray absorption spectroscopy

X-ray absorption measurements were performed at the BM23 beamline of ESRF (Grenoble, France). Ex situ measurements were conducted on pelletized samples of optimal thickness. In situ samples were measured in liquid phase inside a glass cell under controlled temperature and gas atmosphere (Ar or ethylene) with a time resolution of ~90 s per spectrum. The measurements were performed in transmission geometry with the beam intensity registered by ionization chambers. The reference Pd foil was measured simultaneously with the samples for energy calibration. The energy was selected by a Si(111) double-crystal monochromator operated in continuous scanning mode. The rejection of higher harmonics was achieved by Rh-coated mirrors. Processing of the in situ data, multivariate curve resolution analysis and construction of the concentration profiles were performed using the PyFitIt program. Processing of ex situ data and EXAFS fitting were performed with the Demeter package.

Solid-state NMR characterization

Solid-state NMR experiments were performed on a 600-MHz Varian spectrometer, using a 1.6-mm FastMAS probe. Larmor frequencies for ^{27}Al and ^{29}Si were 156.18 MHz and 119.06 MHz, respectively. The samples were spun at 20 kHz. ^{27}Al MAS NMR spectra were recorded with a short 1.0-µs excitation pulse and a recycle delay of 0.1 s. A total of 60,000 scans were recorded per spectrum. In the ^{29}Si MAS NMR experiment, a π/2 pulse of 1.8 µs was used and 1,000 scans were recorded with a recycle delay of 60 s. ^{1}H–^{29}Si cross-polarization (CP) MAS NMR measurements employed a ^{1}H excitation pulse of 1.5 µs and a ramped-amplitude CP block of 4 ms. The delay was 1 s and the number of scans was 40,000. The ^{29}Si spin-lattice relaxation times (T_1) were measured with a saturation recovery pulse sequence. A block of sixty π/2 pulses separated by a rotor period was employed before the magnetization-recovery delay (τ). The recycle delay was 0.1 s and the number of scans was 160.

Scanning electron microscopy

Scanning electron microscopy images were taken using a PHILIPS scanning electron microscope XL30 FEG at an acceleration voltage of 30 kV. Zeolite samples were attached to a piece of carbon tape. Subsequently, a thin Pd/Pt layer was deposited on top of the samples to achieve sufficient conductivity.

ICP

The Pd- and Al contents of zeolites were determined via ICP atomic emission spectroscopy using a Varian 720-ES instrument. Before this, low-boiling organics were evaporated and the zeolites were digested in an HF solution.

Thermogravimetric analysis

Thermogravimetric analysis was performed on a TA Instruments TGA Q500 using an O_2/N_2 gas flow of 2/3 at a heating rate of 3.5 °C min^{-1}.

PXRD

PXRD patterns were recorded on a Malvern PANalytical Empyrean diffractometer equipped with a PIXcel 3D 1 × 1 detector. The powder samples were placed onto a 96-well plate, and patterns were recorded at room temperature in transmission geometry within a 1.3°–50° 2θ range with a step size of 0.013°, and analysed with PANalytical Data Viewer software.

Data availability

The findings of this study are available within the article and its supplementary information. All data are available from the authors upon reasonable request.

References

1. Beller, M., Seayad, J., Tillack, A. & Jiao, H. Catalytic Markovnikov and anti-Markovnikov functionalization of alkenes and alkynes: recent developments and trends. *Angew. Chem. Int. Ed.* **43**, 3368–3398 (2004).
2. Bhawal, B. N. & Morandi, B. Catalytic transfer functionalization through shuttle catalysis. *ACS Catal.* **6**, 7528–7535 (2016).
3. Bhawal, B. N. & Morandi, B. Catalytic isofunctional reactions—expanding the repertoire of shuttle and metathesis reactions. *Angew. Chem. Int. Ed.* **58**, 10074–10103 (2019).
4. Bhawal, B. N. & Morandi, B. Shuttle catalysis—new strategies in organic synthesis. *Chem. A Eur. J.* **23**, 12004–12013 (2017).
5. Fang, X., Yu, P. & Morandi, B. Catalytic reversible alkene-nitrile interconversion through controllable transfer hydrocyanation. *Science* **351**, 832–836 (2016).
6. Fang, X., Cacherat, B. & Morandi, B. CO- and HCl-free synthesis of acid chlorides from unsaturated hydrocarbons via shuttle catalysis. *Nat. Chem.* **9**, 1105–1109 (2017).
7. Murphy, S. K., Park, J. W., Cruz, F. A. & Dong, V. M. Rh-catalyzed C-C bond cleavage by transfer hydroformylation. *Science* **347**, 56–60 (2015).
8. Simonneau, A. & Oestreich, M. 3-silylated cyclohexa-1,4-dienes as precursors for gaseous hydrosilanes: the $B(C_6F_5)_3$-catalyzed transfer hydrosilylation of alkenes. *Angew. Chem. Int. Ed.* **52**, 11905–11907 (2013).
9. Lian, Z., Bhawal, B. N., Yu, P. & Morandi, B. Palladium-catalyzed carbon-sulfur or carbon-phosphorus bond metathesis by reversible arylation. *Science* **356**, 1059–1063 (2017).
10. Mulryan, D., Rodwell, J., Phillips, N. A. & Crimmin, M. R. Au(I) Catalyzed HF transfer: tandem alkyne hydrofluorination and perfluoroarene functionalisation. *ACS Catal* **12**, 3411–3419 (2022).
11. De La Higuera Macias, M. & Arndtsen, B. A. Functional group transposition: a palladium-catalyzed metathesis of Ar-X σ-bonds and acid chloride synthesis. *J. Am. Chem. Soc.* **140**, 10140–10144 (2018).
12. Rong, Z. Q., Lim, H. N. & Dong, G. Intramolecular acetyl transfer to olefins by catalytic C-C bond activation of unstrained ketones. *Angew. Chem. Int. Ed.* **57**, 475–479 (2018).
13. Tan, G., Wu, Y., Shi, Y. & You, J. Syngas-free highly regioselective rhodium-catalyzed transfer hydroformylation of alkynes to α,β-unsaturated aldehydes. *Angew. Chem. Int. Ed.* **58**, 7440–7444 (2019).
14. Yu, P., Bismuto, A. & Morandi, B. Iridium-catalyzed hydrochlorination and hydrobromination of alkynes by shuttle catalysis. *Angew. Chem. Int. Ed.* **59**, 2904–2910 (2020).
15. Li, Y., Bao, G. & Wu, X. F. Palladium-catalyzed intermolecular transthioetherification of aryl halides with thioethers and thioesters. *Chem. Sci.* **11**, 2187–2192 (2020).

16. Delcaillau, T., Boehm, P. & Morandi, B. Nickel-catalyzed reversible functional group metathesis between aryl nitriles and aryl thioethers. *J. Am. Chem. Soc.* **143**, 3723–3728 (2021).
17. Dong, X., Roeckl, J. L., Waldvogel, S. R. & Morandi, B. Merging shuttle reactions and paired electrolysis for reversible vicinal dihalogenations. *Science* **371**, 507–514 (2021).
18. Veth, L., Grab, H. A., Martínez, S., Antheaume, C. & Dydio, P. Transfer C-H borylation of alkenes under Rh(I) catalysis: insight into the synthetic capacity, mechanism and selectivity control. *Chem. Catal.* **2**, 762–778 (2022).
19. Bhunia, A., Bergander, K. & Studer, A. Cooperative palladium/Lewis acid-catalyzed transfer hydrocyanation of alkenes and alkynes using 1-methylcyclohexa-2,5-diene-1-carbonitrile. *J. Am. Chem. Soc.* **140**, 16353–16359 (2018).
20. Bhawal, B. N., Reisenbauer, J. C., Ehinger, C. & Morandi, B. Overcoming selectivity issues in reversible catalysis: a transfer hydrocyanation exhibiting high kinetic control. *J. Am. Chem. Soc.* **142**, 10914–10920 (2020).
21. Luo, X. et al. Mechanism of rhodium-catalyzed formyl activation: a computational study. *J. Org. Chem.* **81**, 2320–2326 (2016).
22. Fürstner, A. Olefin metathesis and beyond. *Angew. Chem. Int. Ed.* **39**, 3012–3043 (2000).
23. Allian, A. D. et al. Process safety in the pharmaceutical industry—Part I: thermal and reaction hazard evaluation processes and techniques. *Org. Process Res. Dev.* **24**, 2529–2548 (2020).
24. Orecchia, P., Yuan, W. & Oestreich, M. Transfer hydrocyanation of α- and α,β-substituted styrenes catalyzed by boron Lewis acids. *Angew. Chem. Int. Ed.* **58**, 3579–3583 (2019).
25. Wang, C. S., Yu, Y., Sunada, Y., Wang, C. & Yoshikai, N. Cobalt-catalyzed carbo- and hydrocyanation of alkynes via C-CN bond activation. *ACS Catal* **12**, 4054–4066 (2022).
26. Landis, C. R. Construction and deconstruction of aldehydes by transfer hydroformylation. *Science* **347**, 29–30 (2015).
27. Wasilke, J. C., Obrey, S. J., Baker, R. T. & Bazan, G. C. Concurrent tandem catalysis. *Chem. Rev.* **105**, 1001–1020 (2005).
28. Frye, N. L., Bhunia, A. & Studer, A. Nickel-catalyzed Markovnikov transfer hydrocyanation in the absence of Lewis acid. *Org. Lett.* **22**, 4456–4460 (2020).
29. Fan, C. & Zhou, Q. L. Nickel-catalyzed group transfer of radicals enables hydrocyanation of alkenes and alkynes. *Chem. Catal.* **1**, 117–128 (2021).
30. Reisenbauer, J. C., Bhawal, B. N., Jelmini, N. & Morandi, B. Development of an operationally simple, scalable and HCN-free transfer hydrocyanation protocol using an air-stable Nickel precatalyst. *Org. Process Res. Dev.* **26**, 1165–1173 (2022).
31. Morandi, B., Fang, Y. & Yu, P. Process for the catalytic reversible alkene-nitrile interconversion. US patent 10,597,356 B2 (2020).
32. Ni, S. F., Yang, T. L. & Dang, L. Transfer hydrocyanation by Nickel(0)/Lewis acid cooperative catalysis, mechanism investigation and computational prediction of shuttle catalysts. *Organometallics* **36**, 2746–2754 (2017).
33. Lenges, C. P. & Brookhart, M. Isomerization of aldehydes catalyzed by rhodium(I) olefin complexes. *Angew. Chem. Int. Ed.* **38**, 3533–3537 (1999).
34. Corma, A. & Iborra, S. Oligomerization of alkenes. *Catal. Fine Chem. Synth.* **4**, 125 (2006).
35. Sanati, M., Hörnell, C. & Järäs, S. G. The oligomerization of alkenes by heterogeneous catalysts. *Catalysis* **14**, 236–288 (2007).
36. Skupińska, J. Oligomerization of α-olefins to higher oligomers. *Chem. Rev.* **91**, 613–648 (1991).
37. Al-Jarallah, A. M., Anabtawi, J. A., Siddiqui, M. A. B., Aitani, A. M. & Al-Sa'doun, A. W. Ethylene dimerization and oligomerization to butene-1 and linear α-olefins. A review of catalytic systems and processes. *Catal. Today* **14**, 1–121 (1992).
38. Ghosh, A. K. & Kevan, L. Catalytic and ESR studies of ethylene dimerization on palladium-exchanged Na-X and Ca-X zeolites. *J. Phys. Chem.* **92**, 4439–4446 (1988).
39. Lallemand, M., Finiels, A., Fajula, F. & Hulea, V. Catalytic oligomerization of ethylene over Ni-containing dealuminated Y zeolites. *Appl. Catal. A Gen.* **301**, 196–201 (2006).
40. O'connor, C. T. & Kojima, M. Alkene oligomerization. *Catal. Today* **6**, 329–349 (1990).
41. Finiels, A., Fajula, F. & Hulea, V. Nickel-based solid catalysts for ethylene oligomerization—a review. *Catal. Sci. Technol.* **4**, 2412–2426 (2014).
42. Wang, S. & Iglesia, E. Mechanism of isobutanal-isobutene Prins condensation reactions on solid Brønsted acids. *ACS Catal.* **6**, 7664–7684 (2016).
43. Arundale, E. & Mikeska, L. A. The olefin-aldehyde condensation. The Prins reaction. *Chem. Rev.* **51**, 505–555 (1952).
44. Vasiliadou, E. S., Li, S., Caratzoulas, S. & Lobo, R. F. Formaldehyde-isobutene Prins condensation over MFI-type zeolites. *Catal. Sci. Technol.* **8**, 5794–5806 (2018).
45. Wilshier, K. G. Propene oligomerization over H-ZSM-5 zeolite. *Stud. Surf. Sci. Catal.* **36**, 621–625 (1988).
46. Sarazen, M. L., Doskocil, E. & Iglesia, E. Effects of void environment and acid strength on alkene oligomerization selectivity. *ACS Catal.* **6**, 7059–7070 (2016).
47. Kuo, T. W. & Tan, C. S. Alkylation of toluene with propylene in supercritical carbon dioxide over chemical liquid deposition HZSM-5 pellets. *Ind. Eng. Chem. Res.* **40**, 4724–4730 (2001).
48. Doyle, M., Us, I. L., Anderson, S. L. & Plaines, D. Alkylation of aromatic hydrocarbons. US patent 4,469,908 (1984).
49. Grigor'eva, N. G., Serebrennikov, D. V., Bubennov, S. V. & Kutepov, B. I. Isoamylene oligomerization over zeolite catalysts. *Pet. Chem.* **61**, 183–189 (2021).
50. Hauge, K., Bergene, E., Chen, D., Fredriksen, G. R. & Holmen, A. Oligomerization of isobutene over solid acid catalysts. *Catal. Today* **100**, 463–466 (2005).
51. Chang, C. D., Chu, C. T. W., Miale, J. N., Bridger, R. F. & Calvert, R. B. Aluminum insertion into high silica zeolite frameworks. 1. Reaction with aluminum halides. *J. Am. Chem. Soc.* **106**, 8143–8146 (1984).
52. Batool, S. R., Sushkevich, V. L. & van Bokhoven, J. A. Correlating Lewis acid activity to extra-framework aluminum species in zeolite Y introduced by ion-exchange. *J. Catal.* **408**, 24–35 (2022).
53. Lang, S. et al. Mechanisms of the $AlCl_3$ modification of siliceous microporous and mesoporous catalysts investigated by multi-nuclear solid-state NMR. *Top. Catal.* **60**, 1537–1553 (2017).
54. Marcilly, C. R. Where and how shape selectivity of molecular sieves operates in refining and petrochemistry catalytic processes. *Top. Catal.* **13**, 357–366 (2000).
55. Csicsery, S. M. Catalysis by shape selective zeolites-science and technology. *Pure Appl. Chem.* **58**, 841–856 (1986).
56. Teketel, S. et al. Shape selectivity in the conversion of methanol to hydrocarbons: the catalytic performance of one-dimensional 10-ring zeolites: ZSM-22, ZSM-23, ZSM-48 and EU-1. *ACS Catal.* **2**, 26–37 (2011).
57. Xue, Y. et al. Enhancing propene selectivity in methanol and/or butene conversion by regulating channel systems over ZSM-5/ZSM-48 composite zeolites. *Microporous Mesoporous Mater.* **312**, 110803 (2021).
58. Bugaev, A. L. et al. The role of palladium carbides in the catalytic hydrogenation of ethylene over supported palladium nanoparticles. *Catal. Today* **336**, 40–44 (2019).

59. Rodriguez-González, L. et al. The acid properties of H-ZSM-5 as studied by NH3-TPD and 27Al-MAS-NMR spectroscopy. *Appl. Catal. A Gen.* **328**, 174–182 (2007).
60. Wagschal, S. et al. Formation of XPhos-ligated palladium(0) complexes and reactivity in oxidative additions. *Chem. Eur. J.* **25**, 6980–6987 (2019).
61. Fang, X., Yu, P., Prina Cerai, G. & Morandi, B. Unlocking Mizoroki-Heck-type reactions of aryl cyanides using transfer hydrocyanation as a turnover-enabling step. *Chem. Eur. J.* **22**, 15629–15633 (2016).
62. Kleemann, A., Engel, J., Kutscher, B. & Reichert, D. *Pharmaceutical Substances* (Thieme, 2011).

Acknowledgements

We thank J. Vercammen for insights on zeolite synthesis and manipulation, K. Lomachenko for help with XAS measurements, G. O'Rourke for assistance with TGA experiments, C. Marquez for help with ICP measurements, and C. Cheung for providing the scanning electron microscopy images. The XAS experiments were performed at beamline BM23 of the European Synchrotron Radiation Facility (ESRF, Grenoble, France). D.D.V. and J.D. are grateful to KULeuven (C1 project) and FWO (G0781118N with ARSS, Slovenia; G0F2320N) for funding. A.K. and G.M. acknowledge financial support from the Slovenian Research Agency (research core funding no. P1-0021 and project no. N1-0079).

Author contributions

D.D.V. and J.D. were responsible for the conception, design and interpretation of the experiments. J.D. and J.W. performed the experiments and analysed the data. J.D., N.V.V. and A.L.B. conceived the design of the XAS experiments, and A.L.B. and O.A.U. were responsible for data processing. A.K. and G.M. conceived and performed the NMR experiments. The paper was written by J.D. and D.D.V., with contributions from all authors.

Competing interests

The authors declare no competing interests.

Additional information

Supplementary information The online version contains supplementary material available at https://doi.org/10.1038/s41929-023-00967-8.

Correspondence and requests for materials should be addressed to Dirk De Vos.

Peer review information *Nature Catalysis* thanks the anonymous reviewers for their contribution to the peer review of this work.